UC Davis

UC Davis Previously Published Works

Title

Influences of Primary Emission and Secondary Coating Formation on the Particle Diversity and Mixing State of Black Carbon Particles

Permalink

https://escholarship.org/uc/item/187872jz

Journal

Environmental Science and Technology, 53(16)

ISSN

0013-936X

Authors

Lee, Alex KY
Rivellini, Laura-Hélèna
Chen, Chia-Li
et al.

Publication Date

2019-08-20

DOI

10.1021/acs.est.9b03064

Peer reviewed

eScholarship.org Powered by the California Digital Library
University of California

Influences of primary emission and secondary coating formation on the particle diversity and mixing state of black carbon particles

Alex K. Y. Lee[1,2*], Laura-Hélèna Rivellini[2], Chia-Li Chen[3^], Jun Liu[3], Derek J. Price[3 ‡], Raghu Betha[3], Lynn M. Russell[3], Xiaolu Zhang[4 #], Christopher D. Cappa[4]

[1]Department of Civil and Environmental Engineering, National University of Singapore, Singapore

[2]NUS Environmental Research Institute, National University of Singapore, Singapore

[3]Scripps Institution of Oceanography, University of California, San Diego, USA

[4]Department of Civil and Environmental Engineering, University of California, Davis, USA

^Now at: Department of Atmospheric Sciences, National Taiwan University, Taipei, Taiwan

‡Now at: Department of Chemistry and Biochemistry, University of Colorado, Boulder, USA

#Now at: Crocker Nuclear Laboratory, University of California, Davis, USA

*Correspondence author

Address:1 Engineering Drive 2, Block E1A #07-03, Singapore, 117576

Email address: ceelkya@nus.edu.sg

Author Version

Abstract

The mixing state of black carbon (BC) affects its environmental fate and impacts. This work investigates particle diversity and mixing state for refractory BC (rBC) containing particles in an urban environment. The chemical compositions of individual rBC-containing particles were measured, from which a mixing state index and particle diversity were determined. The mixing state index (χ) varied between 26 % and 69% with the average of 48% in this study, and was slightly enhanced with the photochemical age of air masses, indicating that most of the rBC-containing particles cannot be simply explained by fully externally and internally mixed model. Clustering of single particle measurements was used to investigate the potential effects of different primary emissions and atmospheric processes on rBC-containing particle diversity and mixing state. The average particle species diversity and the bulk population species diversity both increased with primary traffic emissions and elevated nitrate concentrations in the morning but gradually decreased with secondary organic aerosol (SOA) formation in the afternoon. The single particle clustering results illustrate that primary traffic emissions and entrainment of nitrate-containing rBC particles from the residual layer to the surface could lead to more heterogeneous aerosol compositions, whereas substantial fresh SOA formation near vehicular emissions made the rBC-containing particles more homogeneous. This work highlights the importance of considering particle diversity and mixing state for investigating the chemical evolution of rBC-containing particles and the potential effects of coating on BC absorption enhancement.

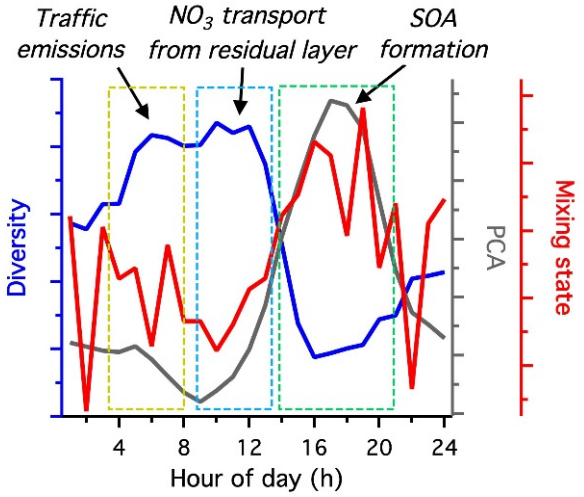

TOC graphic

Author version

1. Introduction

Black carbon (BC) emitted from incomplete combustion affects air quality and climate. BC is the major light absorber in ambient particles, contributing substantially to positive radiative forcing on both regional and global scales.[1, 2] Microscopic imaging techniques have provided direct evidence that BC can be internally mixed with other aerosol species in the atmosphere [3, 4], which can modify the physio-chemical properties of BC-containing particles and hence their environmental fate and impacts.[5-8] In particular, organic aerosol is often internally mixed with BC; this mixing may enhance light absorption of BC particles depending on the degree and types of atmospheric processing.[9-12] While primary organic aerosol (POA) coating can be co-emitted with BC aggregates from combustion processes [3, 4], secondary organic aerosol (SOA) can condense on BC particles, altering BC morphology from highly fractal to compact structures and thus their aerodynamic and deposition characteristics.[11, 13-15]

A parameterization approach has been developed to provide a quantitative description of particle diversity and mixing state.[16-19] This approach requires chemical characterization of atmospheric particles on the single particle level as a model input. However, quantification and characterization of tiny amounts of chemicals in submicron single particle is an analytical challenge. Recent studies have successfully applied different single particle spectro-microscopy techniques to determine the particle mixing state as well as the morphology of carbonaceous and inorganic aerosol components on collection substrates.[18, 20-22] Real-time single particle mass spectrometry is another advanced analytical approach that has been utilized to measure chemical composition of individual particles in urban environments [23-25] and to identify the influence of different anthropogenic emissions and atmospheric processing on the particle diversity and mixing state.[17, 19] Ye et al. [19] recently investigated the evolution of mixing state of primary and secondary aerosol across the urban scale using single particle mass spectroscopy on a mobile platform. They reported that the particle mixing state in the city center showed large spatial heterogeneity that is mostly driven by local emissions, whereas particles were more internally mixed in the upwind and downwind of the urban areas.

Despite the fact that BC particles and its coating compositions can have substantial impacts on the optical and physio-chemical properties of atmospheric particles, our current understanding of BC-containing particles mixing state and their evolution caused by different emissions and atmospheric aging are rather qualitative. Recent development of Aerodyne soot-particle aerosol mass spectrometer (SP-AMS) allows

Author Version

detection of refractory BC (rBC, an operationally defined term[26]) and its associated coating composition exclusively. [27-32] With the single particle characterization capability integrated into the SP-AMS, this study aims to investigate the influence of primary emissions and secondary aerosol species formation on the rBC-containing particle diversity and mixing state near vehicular emission in Fontana, California, which is located in the broader South Coast Air Basin and includes the greater Los Angeles area. While positive matrix factorization (PMF) of ensemble data reported in Lee et al. [28] identified the major sources of BC-containing particles, this work reports new results from cluster analysis of single particle data and particle diversity and mixing state calculation based on the algorithm developed by Reimer and West [16]. The observations provide insight into the chemical evolution of BC-containing particles due to traffic emissions and atmospheric processing and BC absorption enhancement due to the presence of coatings.

2. Experimental Method

2.1 Sampling location and period

Measurements were performed from 5 to 28 July 2015. The sampling site managed by South Coast Air Quality Management District was located at 14360 Arrow Highway in Fontana, California (34.100 N, 117.490 W). The sampling site was surrounded by a few highways and was strongly influenced by vehicular emissions and the broader urban plume. Air pulled through a custom-made isokinetic inlet was dried using diffusion driers and subsequently distributed to different particle instruments. The details of meteorological conditions and other particle instruments have been reported in detail by Chen, et al. [33].This study focuses on the results from a SP-AMS (Aerodyne Research). Two nitrogen oxide analyzers (Model 42i and 42i NO_y, Thermo Fisher Scientific) were used to measure NO_x and NO_y that can be used to calculate photochemical age (PCA) of air masses. The molybdenum converter in the 42i nitrogen oxide analyzer was replaced by an UV-LED photolytic NO_2 converter (Air Quality Design) to improve the accuracy of NO_2 measurement.

2.2 Soot particle aerosol mass spectrometer

The working principle of SP-AMS has been reported by Onasch et al. [26]. The SP-AMS here was operated such that only rBC and non-refractory aerosol species coated on rBC (referred to as NR-PM_{rBC}) are vaporized and detected.[26-32] The resulting vapour is ionized via 70 eV electron impact and then detected by a high-resolution time-of-flight mass spectrometer with a mass resolving power of ~2000 at m/z 28.[34,

Author Version

[35] An efficient particle time-of-flight system (ePToF) was used for measuring aerosol size distributions. The SP-AMS was operated alternating between ensemble mode (i.e., average mass spectrum and PToF size distribution) and event trigger single particle mode (ETSP, i.e., single particle mass spectrum with unit mass resolution (UMR) and PToF size, Section 2.3). Data processing procedures, PMF analysis, calibration, collection efficiency correction and uncertainties of ensemble measurements have been reported in detail by Lee et al. [28]. Note that our calibration and collection efficiency correction approach likely lead to over quantification of the NR-PM_{rBC} mass loadings, representing their upper limits.[24, 28, 36]

2.3 Single particle detection and data processing

The single particle mode (ETSP) has been previously used for investigating sources, atmospheric processing and emission characteristics of aerosol particles.[19, 37-39] The detail of ETSP settings (including the "Region of Interest" (ROI) for trigger detection and the threshold values of each ROI) can be found in the supporting information. Tofware (version 2.4.5) was used to pre-process the ETSP raw data and generate input data for identifying real single particle events using a Cluster Input Preparation Panel (CIPP) as previously described.[24] The CIPP has been used to analyze single particle data measured by Aerodyne AMS equipped with a light scattering module [29, 33, 40, 41] and has been modified to analyze ETSP measurements.[19, 37-39] A simplified version of fragmentation table was used to quantify the ion signals of NR-PM_{rBC} and rBC. The RIE values reported in Lee et al. [28] were used to convert the ion signals to the mass fraction of each chemical component in individual particle. The minimum ion threshold was calculated within the two particle-free d_{va} regions (Figure S2) for identifying real single particle events within the expected d_{va} region (i.e., 50-1200 nm).[42] The output from CIPP was used for performing cluster analysis to investigate the mixing state of all the real particles using a Cluster Analysis Panel (CAP) with the built-in k-means algorithm in IGOR Pro (WaveMetrics Inc., version 6).[24, 29, 40] All single particle mass spectra were normalized by their total ion signal, and solutions with up to 20 clusters were tested. The details of single particle detection and data processing procedure can be found in the supporting information.

2.4 Particle diversity and mixing state calculation

The mass fraction of each chemical component in individual particles and the ensemble-average composition were used to calculate the different diversity parameters and mixing state index (χ) of rBC-containing particles based on the approach described by Riemer and West [16]. Only the four major NR-

Author Version

PM_{rBC} including sulfate, nitrate, ammonium, organic and rBC that can be measured by the SP-AMS were used to determine the number of chemical species for calculating these parameters. The single particle diversity (D_i) characterizes effective number of species in each particle, ranging from 1 to the number of chemical species involved in the calculation, which is equal to 5 in this work. For examples, $D_i = 1$ when the particle consists of a single pure species and $D_i = 5$ when the particle is composed of equal amount of all five species; if the relative abundances of the five components differ the $D_i < 5$.[16] Alpha diversity (D_α) and gamma diversity (D_γ) characterize the average effective number of species in each particle and in the bulk population, respectively. In this work, $D_\alpha = 1$ (i.e., minimum) when all particles are pure and $D_\gamma = 5$ (i.e., maximum) when there are equal bulk mass fractions of all species. D_γ cannot less than D_α, and $D_\alpha = D_\gamma$ when all particles have identical mass fractions.[16] The mixing state index is defined as $(D_\alpha–1)/(D_\gamma–1)$ which measures the homogeneity of the particle population. It ranges from 0% when all particles are pure (i.e., a fully externally mixed population) to 100% when all particles have identical chemical compositions (i.e., a fully internally mixed population).[16]

In this work, the D_i of each individual particle and the corresponding hourly-averaged D_α were calculated from single particle events and the mass fractions of each component in individual particles calculated in the data pre-processing step using CIPP. Hourly-averaged D_γ were calculated using the mass concentration of each chemical species measured in the ensemble mode. In general, the single particle detection efficiency in the ETSP mode decreases with decreasing particle size. The ETSP-derived mass-based size distributions were corrected for the fall off in detection efficiency at smaller sizes for the calculation of D_α (see the supporting information). Figure S4 shows that the hourly-average of the corrected single-particle total signals is strongly correlated with the total mass concentrations of ensemble data ($r^2 = 0.73$). The corrected data was used to calculate the mass fraction of individual particle in the bulk population and subsequently D_α.

3. Results and Discussion

The entire sampling period can be divided into four categories based on the meteorological parameters and anthropogenic activities.[28, 33, 38] As reported in Lee et al. [28], during July 11-17 and 21-28, the weather

Author Version

was relatively hot and dry, referred to as the hot period hereafter. The observations during the hot period show regular diurnal patterns for rBC and NR-PM_{rBC} and will be the focus of the following discussion.

3.1 Overview of SP-AMS ensemble measurement

Figure 1a shows the average diurnal cycles of rBC and NR-PM_{rBC} during the hot period. A detailed discussion of these diurnal patterns was provided by Lee et al. [28]. In brief, the mass loadings of rBC peaked in the morning rush hours mainly due to the combined effects of local traffic emissions, advection, and the rising boundary layer. The diurnal patterns of Organic-to-rBC (Org/rBC) ratio were primarily due to POA co-emitted from nearby traffic in the morning and SOA formation on rBC in the afternoon. In particular, using –log (NO_x/NO_y) as a proxy for the photochemical age (PCA) of air masses (Figure 1b) and Org/rBC as an indicator for SOA formation, fresh SOA coating materials were formed on rBC particles due to active photochemical reactivity of the atmosphere in the afternoon. The secondary nature of organic coatings was supported by the diurnal cycles of O/C, H/C and average carbon oxidation state (OS_c) of total OA (Figure 1c).

Nitrate (NO_3^-) and ammonium (NH_4^+) diurnal patterns correlated strongly with each other, and their mass loadings increased slowly over the night, with more rapid increase after 07:00 local time (LT), and maximum levels at ~10:00–12:00 LT. This behavior could result from time-varying contributions of different NO_3^- formation mechanisms, including daytime photochemically driven production near sources (e.g., OH radical oxidation of NO_2) and nighttime formation (e.g., N_2O_5 chemistry) in the residual layer followed by entrainment of the nitrate-containing rBC particles into the surface mixed layer as the mixed layer height increased. Note that the nighttime formation and particle entrainment mechanism could be more important to explain the observed NO_3^- with relatively large particle size in this work. The decrease of particulate NH_4NO_3 concentrations after noon likely results from the combined effects of boundary layer break up and evaporative loss at the increasing temperature during the day. Sulfate (SO_4^{2-}) remained in low concentrations with a relatively modest pattern. Chloride (Cl^-) also peaked in the morning rush hours and was likely due to condensation of HCl vapor that was subsequently neutralized by NH_3.

3.2 Influence of primary and secondary emissions on particle diversities and mixing state

OA was the dominant component of NR-PM_{rBC}, and hence emissions and atmospheric processes that led to elevated concentrations of any aerosol components other than OA could affect D_α and D_γ. In particular,

Author Version

D_α and D_γ increased with the mass fraction of NO_3^- in rBC-containing particles (Figure 2a), indicating that the NO_3^- and NH_4^+ peaks observed in the morning enhanced the effective number of species in both individual particle and the overall particle population (Figure 1a and b). Furthermore, D_α and D_γ increased with rBC, POA and Cl^- concentrations during the morning rush hours. This result provides direct field evidence that fresh vehicular emissions enhance the diversities of rBC-containing particles although more than one types of particles with different degree of mixing state were likely associated with traffic (see Section 3.3).[24, 28, 29] On the contrary, substantial fresh SOA coating formation coupled with a decrease in the emissions into a larger boundary layer in the afternoon led to reduction of D_α and D_γ, consistent with our observations that formation of other secondary species such as NO_3^- and SO_4^- on rBC particles were small in the afternoon and they only accounted for a small fraction of total NR-PM_{rBC}.

Figure 2b and 2c further illustrates the diurnal changes in D_γ as a function of PCA and coating thickness of rBC ($R_{coat\text{-}BC}$ = NR-PM_{rBC}/rBC from the ensemble data), respectively. Firstly, the PCA remained low between 00:00 and 12:00 LT. The increasing contributions of rBC emissions from traffic (with $R_{coat\text{-}BC} \approx$ 4–5) resulted in a small enhancement of D_γ (starting from 5:00 LT). The value of D_γ remained at ~2.8 until 12:00 LT due to the combined effects of the decreasing concentrations of rBC and the increasing concentrations of NH_4NO_3 (i.e., $R_{coat\text{-}BC}$ increased to ~6). Secondly, D_γ dropped gradually from 2.8 to 2.2 with the increasing PCA, corresponding to the period with significant fresh SOA coating formation in the afternoon (i.e., $R_{coat\text{-}BC}$ increased to ~9). Afterwards, D_γ increased slightly with the decreasing PCA from 18:00 to 00:00 LT. During this period, the SOA coating mass concentrations declined continuously and rBC and other NR-PM_{rBC} species remained in relatively low concentrations (i.e., $R_{coat\text{-}BC}$ decreased to ~4–5). Such observations likely result from the combined effects of reduction of fresh SOA coating formation in the evening, fresh rBC-containing particle emissions into the shallower nocturnal mixed layer and atmospheric dilution by air masses [28, 33] that might carry rBC-containing particle with higher D_γ values (e.g., mixtures of diluted local traffic emissions and aged particles). Figure 2b and 2c summarizes emissions and atmospheric processes that can lead to the observed diurnal variation of D_γ as a function of PCA and $R_{coat\text{-}BC}$, respectively. The similar diurnal changes in D_α in response to PCA was observed.

The mixing state index (χ) was calculated to determine the heterogeneity of the particle population. Figure 2a shows that the hourly-averaged χ varied between 26 % and 69 % with an average of 48% within the

Author Version

hot period. The observed range of χ indicates that the rBC-containing particle population measured during this campaign cannot be simply described by either fully internally (χ = 100%) or externally mixed (χ = 0%) model. The diurnal pattern of χ exhibited an enhancement from ~45% to ~50% when SOA coating formation became more substantial in the afternoon (Figure 1b). Although both NO_3^- and SOA are secondary aerosol species, our results highlight that fresh SOA coating formation could enhance the homogeneity of the rBC-containing particle population (more internally mixed), whereas nitrate-containing rBC particles that were transported from the residual layer to the surface could result in more heterogeneous particle population (more externally mixed). The mixing state showed relatively large deviations during the morning rush hours likely caused by more diverse particle types emitted from traffic. The characteristics of specific particle types that were associated with NO_3^- and SOA coating formation and primary traffic emissions will be discussed in Section 3.3.

3.3 Identification of particle types and their connection to the observed particle diversities

Seven types of particle were identified based on the clustering of ETSP measurements (Figure 3). These are used to further investigate the potential impacts of specific particle emissions and secondary aerosol formation mechanisms to the observed particle diversities and mixing states. Three particle types, referred to as HOA (hydrocarbon-like OA), rBC and K (potassium) classes, that were mainly originated from primary traffic emissions (i.e., the morning rush hour peaks) were observed. Their diurnal cycles (Figure 3o, p and q) were consistent with those of HOA- and rBC-rich factors determined from the PMF analysis of ensemble measurements.[28] While the mass spectrum of HOA-class particles was dominated by the hydrocarbon fragments (e.g., $C_xH_y^+$ at m/z 41, 43, 55, 57) and was similar to that of HOA-rich factor, the rBC and K classes comprised more refractory carbon (e.g., C_x^+ at m/z 12, 24, 36) and perhaps oxygenated organic fragments indicated by the relatively strong ion signals at m/z 43 (i.e., $C_2H_3O^+$ and $C_3H_7^+$) without noticeable hydrocarbon pattern. The rBC-rich factor were also composed of more oxygenated fragments compared to the HOA-rich factor due to the presence of $C_2H_3O^+$ organic fragments and refractory ion fragments (i.e., CO^+ and CO_2^+) [28] that originated from oxygenated functionalities of soot particles.[43, 44] The rBC particle class exhibited the smallest d_{va} among the three traffic-related particle classes. Note that the rBC and HOA particle classes have been reported in previous urban studies using a SP-AMS equipped with a light scattering module for single particle characterizations.[24, 29]

Author Version

The remaining four clusters represent particle types that were associated with secondary aerosol formation and processing, referred to as NO_3, SO_4, OOA and HMW classes hereafter. PMF analysis of the ensemble measurements yielded two oxygenated organic aerosol (OOA) factors, namely OOA-1 and OOA-2.[28] The NO_3 class shows distinct diurnal pattern that is generally consistent with the bulk observation of NO_3^-, although with a notably sharper peak (Figure 3t). More importantly the NO_3 class was an internal mixture of NO_3^- and oxygenated organics, which can partially explain the elevated mass loadings of NO_3^- and OOA-1 factor at 10:00-11:00 LT (Figure 3r and t). The OOA class likely represented the freshly formed SOA in the afternoon, giving its diurnal profile and mass spectral characteristics similar to the OOA-2 factor (Figure 3s). There was a particle class composed of a large fraction of high molecular weight fragments (HMW class) having a diurnal pattern similar to the OOA-1 factor (Figure 3d and r). Nevertheless, OOA-1 likely represented SOA component, whereas the HMW class could be the mixture of POA and SOA materials as indicated by its strong signal at m/z 43 and regular hydrocarbon pattern within larger m/z range. Lastly, SO_4 class was largely internally mixed with OOA and HMW organics but did not give clear diurnal variations.

The single particle diversity (D_i) were calculated to determine effective number of species in each detected particle. The diurnal variations of D_α and D_i matched well with each other (Figure 1b), suggesting that the averaged D_i value of an individual particle class can be used to interpret the diurnal pattern of D_α and D_γ. The average and distributions of D_i of the seven particle classes are presented in Figure 4c. The rBC, K and NO_3 classes have the relatively high average D_i values (1.90–2.60) compared to other particle types (1.44–1.64) in which OA contributed to 79–86% of individual particle mass on average. NO_3 class has the largest D_i which matched with the observation that the elevated NO_3^- concentrations observed in this work could enhance both D_α and D_γ. The aerosol species other than OA accounted for ~50% of individual particle on average within the NO_3 class (Figure 4a). Four particle types (i.e., HOA, rBC, K and a fraction of HMW classes) were associated with the local traffic emissions but their relative contributions might vary from different types of vehicles (e.g., fuel and engine types) that requires further investigation. Their D_i values indicate that rBC and K particle classes (2.08 and 1.90) had more heterogeneous aerosol composition than the HOA and HMW classes (1.46 and 1.44). Furthermore, the HMW and OOA classes had relatively small average values of D_i, suggesting that the fresh SOA materials coated on rBC were the key contributors to make the individual and overall particle composition more homogeneous in the afternoon.

Author Version

Figure 5 shows the image plot and the average values of D_i within specific d_{va} bin width. Although the average D_i values varied between different particle types as shown in Figure 4, there was a weak size dependence of D_i. One of the major reasons for this observation is that the size distributions of each particle type were overlapped significantly (Figure 3). In general, rBC-containing particle associated with secondary aerosol species had larger particle diameter. While rBC and K classes enhance the average D_i within the smaller particle range (e.g., d_{va} < 100 nm), the NO_3 class particles resulted in the increasing average values of D_i for the relatively large particle size (e.g., d_{va} > 400 nm) as shown in Figure 5a. Healy et al [17] observed the similar size dependence of D_i in Paris due to higher fractions of BC and NO_3^- in smaller and larger particle size ranges, respectively. The lowest average D_i values were observed at ~200 nm. This was mainly due to the fact that the size distribution of HOA, OOA and HMW classes, which had relative low value of D_i as shown in Figure 4, peaked at the similar range of d_{va}. These observations indicate that the size-resolve D_i and perhaps mixing state depends on the types of particle emissions, formation mechanisms and atmospheric aging.

The rBC coating thickness ($R_{coat\text{-}BC}$) of each particle type and how they varied as particle size within specific particle types are presented in Figure 4b and 5b, respectively. The $R_{coat\text{-}BC}$ is a parameter commonly used to evaluate the impacts of coating materials on the BC absorption enhancement[4, 10, 45]. Note that some particles did not contain detectable levels of rBC and they were excluded in the $R_{coat\text{-}BC}$ calculation. The size dependence of $R_{coat\text{-}BC}$ within individual particle type is characterized by calculating the average $R_{coat\text{-}BC}$ within specific particle size bins (bin width = 50 nm for d_{va} between 50 and 1000 nm) for all bins that contained more than 50 particles with detectable rBC ion signals were reported. The rBC class particles had the lowest average $R_{coat\text{-}BC}$ of ~0.6 among the identified particle types, followed by the K class particles (4.0). The $R_{coat\text{-}BC}$ of other particle types ranged between 5.9 and 9.1 on average (Figure 4b).

The rBC class particles only exhibited small variation of $R_{coat\text{-}BC}$ (~0.5–0.7) between 50 and 300 nm d_{va} (Figure 5b). While the absolute concentration of the rBC-class particles was similar to or smaller than the other particle types, rBC made up a much larger fraction of the rBC class particle mass. In addition, rBC-class particles were smaller than other particle types, likely resulting in a lower detection efficiency. Thus, the rBC-class particles contain a large fraction of the total rBC mass and, consequently, these particles

Author Version

have a disproportionate influence on the total absorption. Liu et al.[12] reported that the thinly coated rBC-containing particles from fresh traffic emissions (i.e., with M_p = non-BC/BC ratio < 1.5) exhibit unexpectedly small, near unity rBC absorption enhancements. Since traffic emission was the major source of rBC in this field campaign[28], the low $R_{coat\text{-}BC}$ for rBC particle class might be able to explain the overall very small rBC absorption enhancement reported by Cappa et al[45]. If Cappa et al[45] assumed an absorption enhancement of unity for the rBC-rich particles, rather than 1.45, their calculated ensemble-average enhancement would be reduced from ca. 1.75 to ca. 1.45. This calculated value is more in line with their observation of an absorption enhancement of 1.07, but still elevated. It may be that additional, unresolved particle diversity impacts the absorption enhancement.[46]

For all non-rBC class particles (i.e., all particle classes identified in this work except the rBC class), the $R_{coat\text{-}BC}$ increases with particle size, indicating an increase in the coating thickness with the rBC core size. Such behavior contrasts with that expected for diffusion-controlled growth onto a polydisperse distribution of particles, for which coating thickness decreases with core size.[47] The apparent increases with size here are likely artifacts of the event-trigger single particle method (see Section 3.4), which tends to produce too-high $R_{coat\text{-}BC}$ values compared to the ensemble measurements and limits the determination of the specific behavior for the non-rBC class particles. Nonetheless, the non-rBC class particles all clearly have $R_{coat\text{-}BC}$ much larger than the rBC class particles, and potentially >3 across a broad range of sizes. Wu et al.[48] quantified rBC absorption enhancement using a theoretical model parametrized by the complex particle morphology of BC in different aging scales, concluding that rBC absorption enhancement rapidly increase with M_p between 1 and 200. Furthermore, Liu et al.[12] reported that ambient particles with $M_p > 3$ start to show observable impacts on rBC absorption enhancement, suggesting a notable absorption enhancement could have occurred for these non-rBC class particles. However, even at larger coating thicknesses Liu et al.[12] observed a depression of the absorption enhancement relative to core-shell Mie theory. This could further help explain the remaining discrepancy between the Cappa et al[45] observations and calculated absorption enhancements.

3.4 Limitation and recommendations

There are a few limitations of this single particle technology that requires further development. Firstly, the current calibration is based on the comparison between signals from the SP-AMS and an external

Author Version

particle counter that depends on the degree of particle beam and laser vaporizer overlapping within the instrument.[36, 49] This technical limitation is related to the collection efficiency issue of rBC and can be avoided using the ETSP mode for calibration, which is under investigation in our laboratory. Secondly, the relative number distribution and the mass spectral features of different particle types can be affected by m/z assigned in each ROI. For example, some rBC-containing particles did not give detectable levels (or only gave weak levels) of rBC ion signals due to the ROI setting that targeted nitrate- and organic-containing particles (see the supporting information), resulting in overestimating the $R_{coat\text{-}BC}$ and underestimating the D_i of individual particle, especially for the non-rBC class particles. More laboratory and field investigations are required to better understand the potential measurement bias due to the ROI settings. Thirdly, POA and SOA can be internally mixed. The PMF analysis can separate total OA into a few OA types. Performing clustering of single particle data may be able to further separate POA and SOA components in the HMW class but the data interpretation become increasingly subjective. Separation of various POA and SOA species within a single particle can certainly enhance our understanding on the influence of the different primary and secondary emissions on the evolution of rBC-containing particles. Since the current clustering is based on UMR mass spectral data, development of data analysis approach for pre-processing high-resolution mass spectrometric single particle data may improve the performance of clustering and allows elemental analysis for characterizing the mixing of POA and SOA within individual particle.

4. Atmospheric implications

This work identifies a few key processes that likely govern the observed diurnal patterns of particle diversities of rBC-containing particles in summertime Fontana, CA based on single particle measurements made using an SP-AMS (Figure 2b and 2c). They are (1) rBC emissions from traffic and nitrate entrainment from residual layer in the morning (2) fresh SOA formation in the afternoon, and (3) primary traffic emissions with the influence of atmospheric dilution that carried regional background particles to the site. In particular, we provide evidence that fresh SOA formation near vehicular emissions could enhance the homogeneity of the rBC-containing particles (i.e., higher χ), whereas the elevated nitrate concentrations in the late morning resulted in relatively heterogeneous aerosol composition. The D_i of individual particle type illustrates that rBC and K particle classes emitted from traffic led to more heterogeneous aerosol composition but the overall effects on mixing state might be cancelled out by the

Author Version

co-emitted HOA and HMW particle classes, which were largely dominated by OA. The clustering results also enhance our understanding of the size-dependent particle diversity.

The evolution of rBC-containing particles in urban environment involves complex atmospheric processing. Our observations demonstrate the unique research capability for evaluating how the particle diversities and mixing state in response to individual type of particles originated from different primary and secondary sources. The data output from our approach can be used as inputs to measurement-constrained models to evaluate the chemical evolution and the changes in physio-chemical properties of rBC-containing particles including cloud condensation nuclei (CCN) activity and optical properties under different scenarios of atmospheric processing.[16, 29, 50] Recent studies have shown that size-resolved and particle-level chemical composition are particularly important for predicting CCN activity in aerosol populations that are more externally mixed[50] or strongly influenced by local emissions.[51] Fierce et al.[46] showed that light absorption of BC can be overestimated by up to a factor of two by assuming population-averaged composition across all BC-containing particles and neglecting particle diversity using a particle-resolved aerosol model. Cappa et al. [45] also highlighted the importance of particle-to-particle and/or size dependent diversity to explain the discrepancy of rBC absorption enhancement between field observations and theoretical calculations. Liu et al.[12] recently demonstrated that the occurrence of the BC absorption enhancement can be determined based on the M_p (i.e., non-BC/BC) ratio of aerosol particles. However, this work reports that the particle diversity can vary between different particle types and size regardless if they are formed or emitted from the similar source or not. Except for the rBC particle class, the coating thickness ($R_{coat\text{-}BC}$, i.e. a parameter that is equivalent to M_p) showed similar particle size dependence for other particle types. Overall, the single particle mass spectrometry technique used in this study has a great potential to improve our understanding of CCN activation and absorption enhancement of rBC due to the presence of coating as the influences of emissions and atmospheric processes on the $R_{coat\text{-}BC}$, chemical composition and particle diversity (Figure 4b and 4c) on specific particles types and size can be better described in model simulations.

Author Version

Acknowledgements: Lee A. K. Y. and Rivellini L.-H. would like to acknowledge the support from the NUS Start-up Grant (R-302-000-173-133). Cappa D. C. and Russell L. M. were supported by the California Air Resources Board (Agreement number: 13-330). The authors would also like to thank the Fontana Fire Department and the South Coast Air Quality Management District (SCAQMD) for Fontana site logistics.

Supporting information: Detail description of single particle detection and data analysis, Figure S1-S4.

Author Version

Figures and Captions

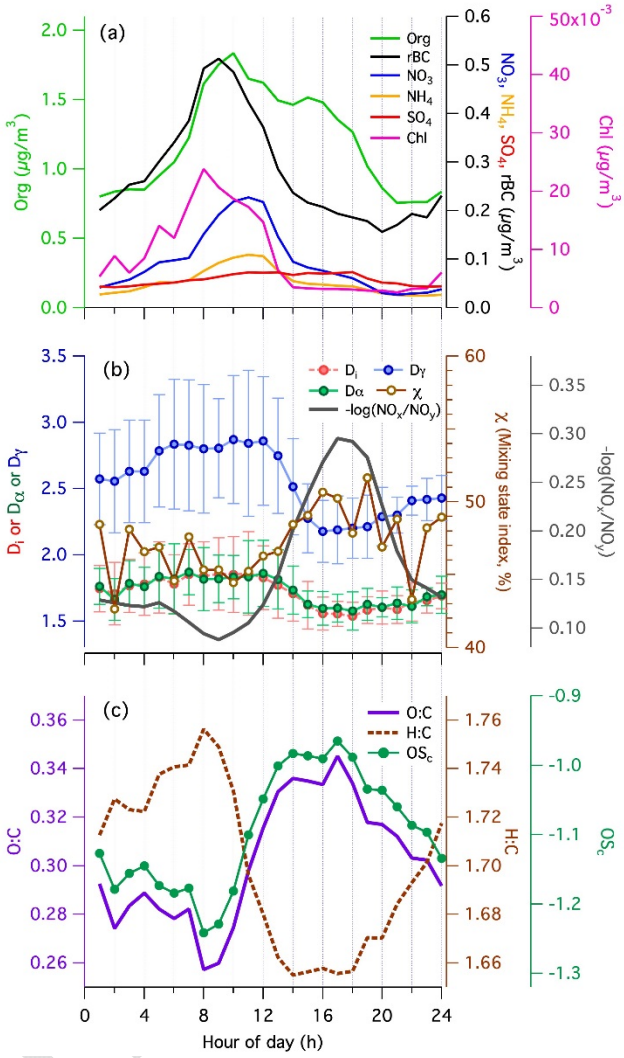

Figure 1: Diurnal patterns of (a) rBC and NR-PM_{rBC}, (b) particle diversities (D_i, D_α and D_γ), mixing state index (χ) and -log(NO_x/NO_y), and (c) elemental ratio (i.e., O:C and H:C) and carbon oxidation state (OS_c) during the hot period.

Author Version

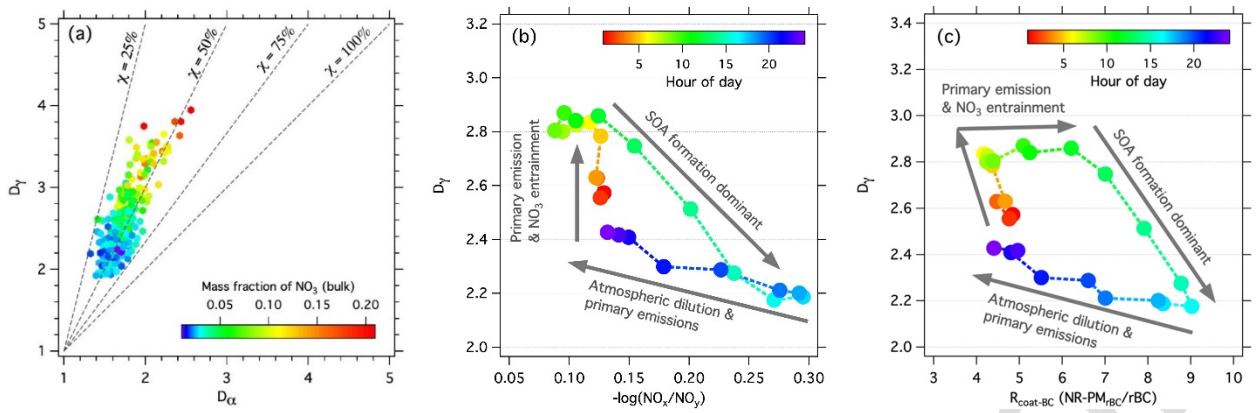

Figure 2: (a) Mixing state diagram showing the normalized population species diversity (D_γ) versus the normalized average particle species diversity (D_α). The dashed lines represent different degree of mixing (χ = 25, 50, 75, and 100%). Changes in D_γ as a function of (b) PCA and (c) $R_{coat\text{-}BC}$ (=NR-PM_{rBC}/rBC from ensemble data) due to different physical and chemical processing of rBC containing particles.

Author Version

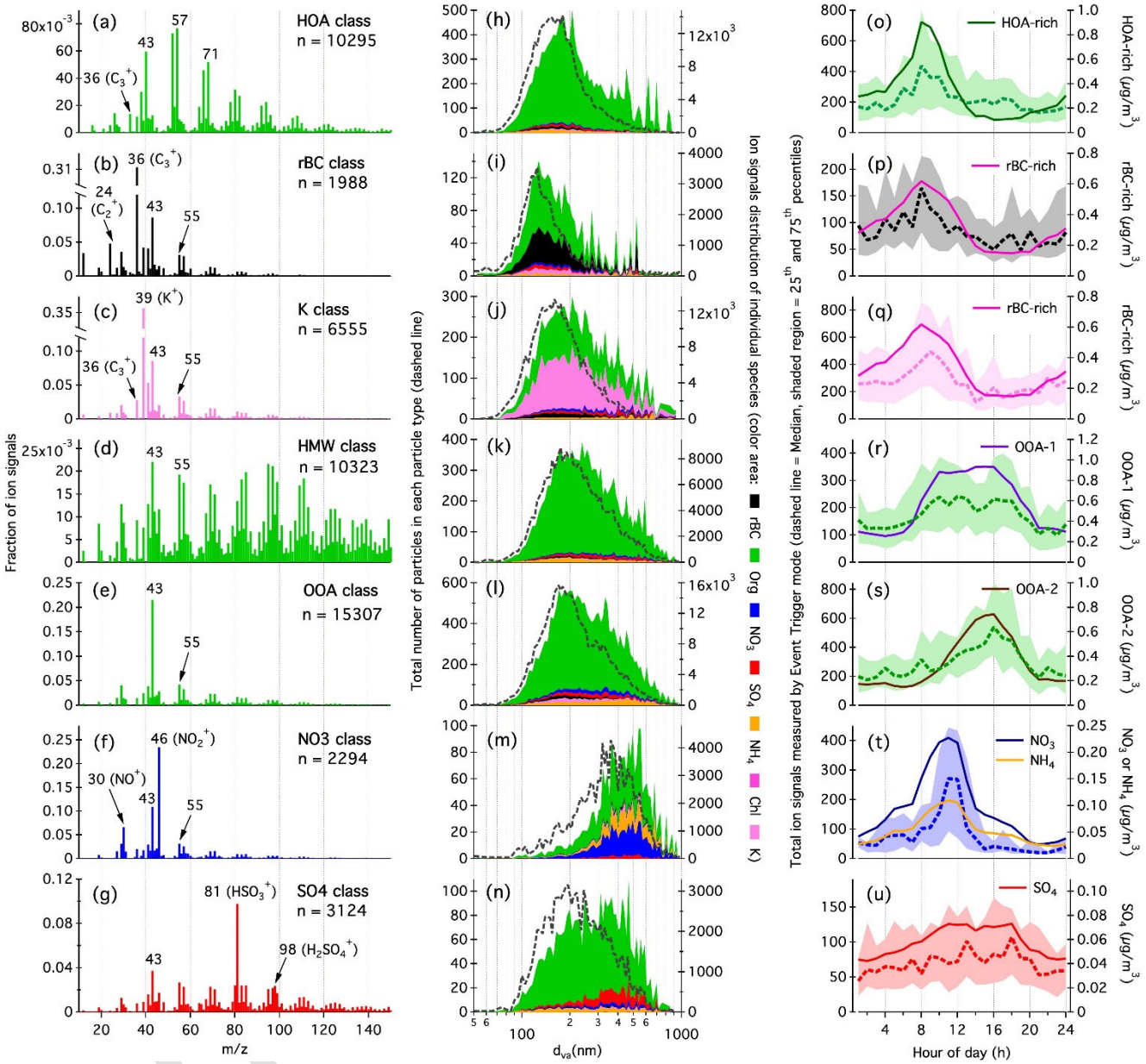

Figure 3: Mass spectra (a-g), size distributions of particle number and ion signal (h-n), and diurnal patterns (o-u) of individual particle types determined by the cluster analysis of ESTP data, NR-PM_{rBC} and PMF factors.

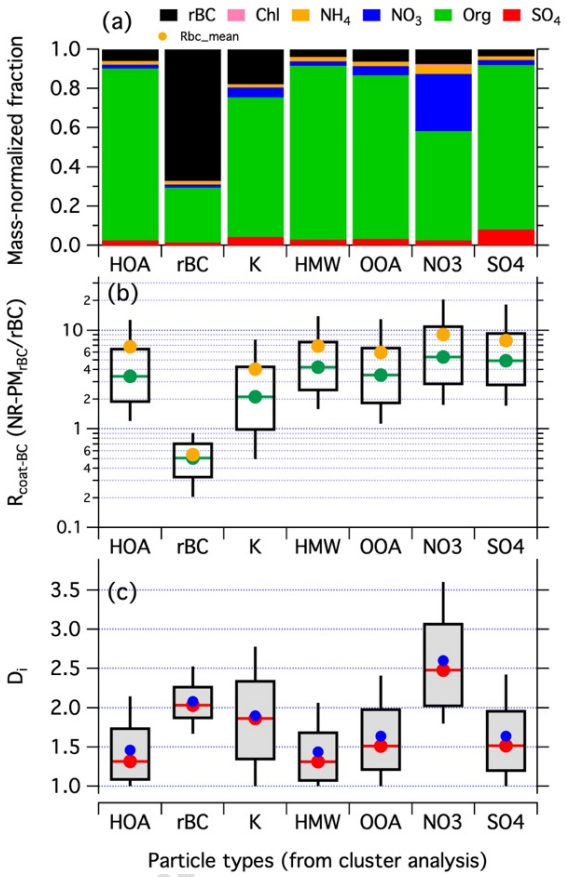

Figure 4: (a) Average mass fraction of individual particle type. (b) Box plots of $R_{coat\text{-}BC}$ of individual particle type (10^{th}, 25^{th}, 75^{th} and 90^{th} percentiles). The green and orange circles represent the mean and the 50^{th} percentile of $R_{coat\text{-}BC}$, respectively. (c) Box plots of D_i of individual particle type (10^{th}, 25^{th}, 75^{th} and 90^{th} percentiles). The blue and red circles represent the mean and the 50^{th} percentile of D_i, respectively.

Author version

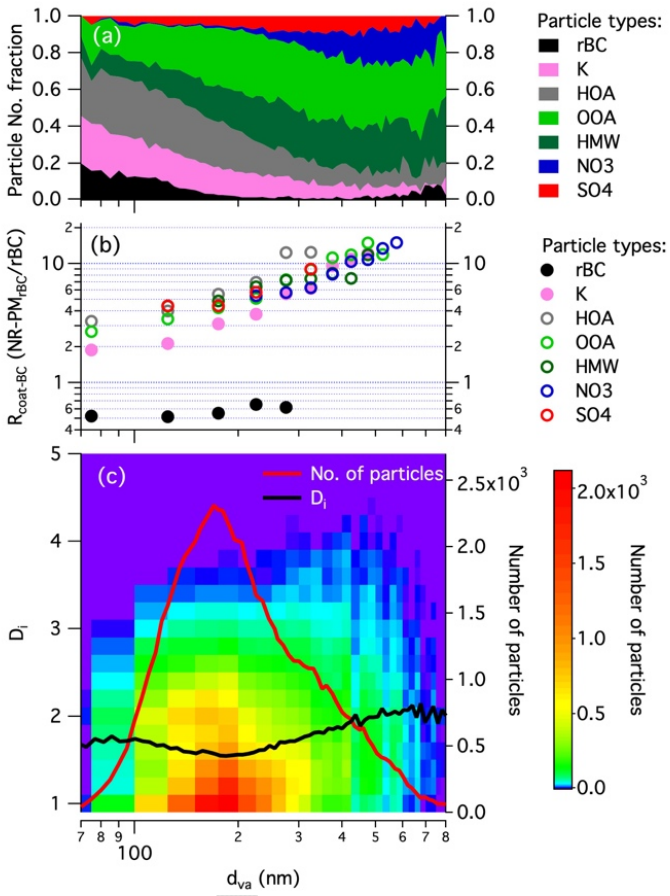

Figure 5: (a) Particle number fraction of particle types as a function of particle size distribution. (b) The average of $R_{coat-BC}$ of individual particle type as a function of particle size distribution. R_{BC} only reported for particle size bins (bin width = 50 nm) containing more than 50 particles with detectable rBC ion signals. (c) Image plot of D_i as a function of particle size distributions. The red and black lines represent the average D_i as a function of particle size and particle number size distribution, respectively.

Author version

References

1. Ramanathan, V.; Carmichael, G., Global and regional climate changes due to black carbon. *Nat. Geosci.* **2008,** *1*, (4), 221-227.

2. Bond, T. C.; Doherty, S. J.; Fahey, D. W.; Forster, P. M.; Berntsen, T.; DeAngelo, B. J.; Flanner, M. G.; Ghan, S.; Karcher, B.; Koch, D.; Kinne, S.; Kondo, Y.; Quinn, P. K.; Sarofim, M. C.; Schultz, M. G.; Schulz, M.; Venkataraman, C.; Zhang, H.; Zhang, S.; Bellouin, N.; Guttikunda, S. K.; Hopke, P. K.; Jacobson, M. Z.; Kaiser, J. W.; Klimont, Z.; Lohmann, U.; Schwarz, J. P.; Shindell, D.; Storelvmo, T.; Warren, S. G.; Zender, C. S., Bounding the role of black carbon in the climate system: A scientific assessment. *Journal of Geophysical Research-Atmospheres* **2013,** *118*, (11), 5380-5552.

3. China, S.; Mazzoleni, C.; Gorkowski, K.; Aiken, A. C.; Dubey, M. K., Morphology and mixing state of individual freshly emitted wildfire carbonaceous particles. *Nature Communications* **2013,** *4*, 2122.

4. Liu, S.; Aiken, A. C.; Gorkowski, K.; Dubey, M. K.; Cappa, C. D.; Williams, L. R.; Herndon, S. C.; Massoli, P.; Fortner, E. C.; Chhabra, P. S.; Brooks, W. A.; Onasch, T. B.; Jayne, J. T.; Worsnop, D. R.; China, S.; Sharma, N.; Mazzoleni, C.; Xu, L.; Ng, N. L.; Liu, D.; Allan, J. D.; Lee, J. D.; Fleming, Z. L.; Mohr, C.; Zotter, P.; Szidat, S.; Prevot, A. S. H., Enhanced light absorption by mixed source black and brown carbon particles in UK winter. *Nature Communications* **2015,** *6*, 8435.

5. Kuwata, M.; Kondo, Y.; Takegawa, N., Critical condensed mass for activation of black carbon as cloud condensation nuclei in Tokyo. *Journal of Geophysical Research-Atmospheres* **2009,** *114*, D20202.

6. McMeeking, G. R.; Good, N.; Petters, M. D.; McFiggans, G.; Coe, H., Influences on the fraction of hydrophobic and hydrophilic black carbon in the atmosphere. *Atmospheric Chemistry and Physics* **2011,** *11*, (10), 5099-5112.

7. Laborde, M.; Crippa, M.; Tritscher, T.; Juranyi, Z.; Decarlo, P. F.; Temime-Roussel, B.; Marchand, N.; Eckhardt, S.; Stohl, A.; Baltensperger, U.; Prevot, A. S. H.; Weingartner, E.; Gysel, M., Black carbon physical properties and mixing state in the European megacity Paris. *Atmospheric Chemistry and Physics* **2013,** *13*, (11), 5831-5856.

8. Liu, D.; Allan, J.; Whitehead, J.; Young, D.; Flynn, M.; Coe, H.; McFiggans, G.; Fleming, Z. L.; Bandy, B., Ambient black carbon particle hygroscopic properties controlled by mixing state and composition. *Atmospheric Chemistry and Physics* **2013,** *13*, (4), 2015-2029.

9. Jacobson, M. Z., Strong radiative heating due to the mixing state of black carbon in atmospheric aerosols. *Nature* **2001,** *409*, (6821), 695-697.

10. Cappa, C. D.; Onasch, T. B.; Massoli, P.; Worsnop, D. R.; Bates, T. S.; Cross, E. S.; Davidovits, P.; Hakala, J.; Hayden, K. L.; Jobson, B. T.; Kolesar, K. R.; Lack, D. A.; Lerner, B. M.; Li, S. M.; Mellon, D.; Nuaaman, I.; Olfert, J. S.; Petaja, T.; Quinn, P. K.; Song, C.; Subramanian, R.; Williams, E. J.; Zaveri, R. A., Radiative Absorption Enhancements Due to the Mixing State of Atmospheric Black Carbon. *Science* **2012,** *337*, (6098), 1078-1081.

11. Peng, J. F.; Hu, M.; Guo, S.; Du, Z. F.; Zheng, J.; Shang, D. J.; Zamora, M. L.; Zeng, L. M.; Shao, M.; Wu, Y. S.; Wang, Y.; Glen, C. R.; Collins, D. R.; Molina, M. J.; Zhang, R. Y., Markedly enhanced absorption and direct radiative forcing of black carbon under polluted urban environments. *Proceedings of the National Academy of Sciences of the United States of America* **2016,** *113*, (16), 4266-4271.

12. Liu, D. T.; Whitehead, J.; Alfarra, M. R.; Reyes-Villegas, E.; Spracklen, D. V.; Reddington, C. L.; Kong, S. F.; Williams, P. I.; Ting, Y. C.; Haslett, S.; Taylor, J. W.; Flynn, M. J.; Morgan, W. T.; McFiggans, G.; Coe, H.; Allan, J. D., Black-carbon absorption enhancement in the atmosphere determined by particle mixing state. *Nat. Geosci.* **2017,** *10*, (3), 184-U132.

Author version

13. Moffet, R. C.; Prather, K. A., In-situ measurements of the mixing state and optical properties of soot with implications for radiative forcing estimates. *Proceedings of the National Academy of Sciences of the United States of America* **2009,** *106*, (29), 11872-11877.

14. Schnitzler, E. G.; Dutt, A.; Charbonneau, A. M.; Olfert, J. S.; Jager, W., Soot Aggregate Restructuring Due to Coatings of Secondary Organic Aerosol Derived from Aromatic Precursors. *Environmental Science & Technology* **2014,** *48*, (24), 14309-14316.

15. Guo, S.; Hu, M.; Lin, Y.; Gomez-Hernandez, M.; Zamora, M. L.; Peng, J. F.; Collins, D. R.; Zhang, R. Y., OH-Initiated Oxidation of m-Xylene on Black Carbon Aging. *Environmental Science & Technology* **2016,** *50*, (16), 8605-8612.

16. Riemer, N.; West, M., Quantifying aerosol mixing state with entropy and diversity measures. *Atmos Chem Phys* **2013,** *13*, (22), 11423-11439.

17. Healy, R. M.; Riemer, N.; Wenger, J. C.; Murphy, M.; West, M.; Poulain, L.; Wiedensohler, A.; O'Connor, I. P.; McGillicuddy, E.; Sodeau, J. R.; Evans, G. J., Single particle diversity and mixing state measurements. *Atmos Chem Phys* **2014,** *14*, (12), 6289-6299.

18. O'Brien, R. E.; Wang, B.; Laskin, A.; Riemer, N.; West, M.; Zhang, Q.; Sun, Y.; Yu, X.-Y.; Alpert, P.; Knopf, D. A.; Gilles, M. K.; Moffet, R. C., Chemical imaging of ambient aerosol particles: Observational constraints on mixing state parameterization. *Journal of Geophysical Research: Atmospheres* **2015,** *120*, (18), 9591-9605.

19. Ye, Q.; Gu, P.; Li, H. Z.; Robinson, E. S.; Lipsky, E.; Kaltsonoudis, C.; Lee, A. K. Y.; Apte, J. S.; Robinson, A. L.; Sullivan, R. C.; Presto, A. A.; Donahue, N. M., Spatial Variability of Sources and Mixing State of Atmospheric Particles in a Metropolitan Area. *Environ Sci Technol* **2018,** *52*, (12), 6807-6815.

20. Ault, A. P.; Axson, J. L., Atmospheric Aerosol Chemistry: Spectroscopic and Microscopic Advances. *Analytical Chemistry* **2017,** *89*, (1), 430-452.

21. Bondy, A. L.; Bonanno, D.; Moffet, R. C.; Wang, B.; Laskin, A.; Ault, A. P., The diverse chemical mixing state of aerosol particles in the southeastern United States. *Atmos Chem Phys* **2018,** *18*, (16), 12595-12612.

22. Moffet, R. C.; O'Brien, R. E.; Alpert, P. A.; Kelly, S. T.; Pham, D. Q.; Gilles, M. K.; Knopf, D. A.; Laskin, A., Morphology and mixing of black carbon particles collected in central California during the CARES field study. *Atmos Chem Phys* **2016,** *16*, (22), 14515-14525.

23. Moffet, R. C.; de Foy, B.; Molina, L. T.; Molina, M. J.; Prather, K. A., Measurement of ambient aerosols in northern Mexico City by single particle mass spectrometry. *Atmos Chem Phys* **2008,** *8*, (16), 4499-4516.

24. Lee, A. K. Y.; Willis, M. D.; Healy, R. M.; Onasch, T. B.; Abbatt, J. P. D., Mixing state of carbonaceous aerosol in an urban environment: single particle characterization using the soot particle aerosol mass spectrometer (SP-AMS). *Atmospheric Chemistry and Physics* **2015,** *15*, (4), 1823-1841.

25. Pratt, K. A.; Prather, K. A., Real-Time, Single-Particle Volatility, Size, and Chemical Composition Measurements of Aged Urban Aerosols. *Environ Sci Technol* **2009,** *43*, (21), 8276-8282.

26. Onasch, T. B.; Trimborn, A.; Fortner, E. C.; Jayne, J. T.; Kok, G. L.; Williams, L. R.; Davidovits, P.; Worsnop, D. R., Soot Particle Aerosol Mass Spectrometer: Development, Validation, and Initial Application. *Aerosol Science and Technology* **2012,** *46*, (7), 804-817.

27. Collier, S.; Williams, L. R.; Onasch, T. B.; Cappa, C. D.; Zhang, X.; Russell, L. M.; Chen, C.-L.; Sanchez, K. J.; Worsnop, D. R.; Zhang, Q., Influence of Emissions and Aqueous Processing on Particles Containing Black Carbon in a Polluted Urban Environment: Insights From a Soot Particle-Aerosol Mass Spectrometer. *Journal of Geophysical Research: Atmospheres* **2018,** *123*, (12), 6648-6666.

Author Version

519 28. Lee, A. K. Y.; Chen, C. L.; Liu, J.; Price, D. J.; Betha, R.; Russell, L. M.; Zhang, X.; Cappa, C. D., Formation of
520 secondary organic aerosol coating on black carbon particles near vehicular emissions. *Atmos Chem Phys* **2017,** *17*, (24),
521 15055-15067.

522 29. Willis, M. D.; Healy, R. M.; Riemer, N.; West, M.; Wang, J. M.; Jeong, C. H.; Wenger, J. C.; Evans, G. J.; Abbatt, J. P.
523 D.; Lee, A. K. Y., Quantification of black carbon mixing state from traffic: implications for aerosol optical properties.
524 *Atmospheric Chemistry and Physics* **2016,** *16*, (7), 4693-4706.

525 30. Wang, J.; Liu, D.; Ge, X.; Wu, Y.; Shen, F.; Chen, M.; Zhao, J.; Xie, C.; Wang, Q.; Xu, W.; Zhang, J.; Hu, J.; Allan, J.;
526 Joshi, R.; Fu, P.; Coe, H.; Sun, Y., Characterization of black carbon-containing fine particles in Beijing during
527 wintertime. *Atmos Chem Phys* **2019,** *19*, (1), 447-458.

528 31. Massoli, P.; Fortner, E. C.; Canagaratna, M. R.; Williams, L. R.; Zhang, Q.; Sun, Y.; Schwab, J. J.; Trimborn, A.;
529 Onasch, T. B.; Demerjian, K. L.; Kolb, C. E.; Worsnop, D. R.; Jayne, J. T., Pollution Gradients and Chemical
530 Characterization of Particulate Matter from Vehicular Traffic near Major Roadways: Results from the 2009 Queens
531 College Air Quality Study in NYC. *Aerosol Sci Technol* **2012,** *46*, (11), 1201-1218.

532 32. Massoli, P.; Onasch, T. B.; Cappa, C. D.; Nuamaan, I.; Hakala, J.; Hayden, K.; Li, S. M.; Sueper, D. T.; Bates, T. S.;
533 Quinn, P. K.; Jayne, J. T.; Worsnop, D. R., Characterization of black carbon-containing particles from soot particle
534 aerosol mass spectrometer measurements on the R/V Atlantis during CalNex 2010. *J Geophys Res Atmos* **2015,** *120*, (6),
535 2575-2593.

536 33. Chen, C.-L.; Chen, S.; Russell, L. M.; Liu, J.; Price, D. J.; Betha, R.; Sanchez, K. J.; Lee, A. K. Y.; Williams, L.;
537 Collier, S. C.; Zhang, Q.; Kumar, A.; Kleeman, M. J.; Zhang, X.; Cappa, C. D., Organic Aerosol Particle Chemical
538 Properties Associated With Residential Burning and Fog in Wintertime San Joaquin Valley (Fresno) and With Vehicle
539 and Firework Emissions in Summertime South Coast Air Basin (Fontana). *Journal of Geophysical Research:*
540 *Atmospheres* **2018,** *123*, (18), 10,707-10,731.

541 34. DeCarlo, P. F.; Kimmel, J. R.; Trimborn, A.; Northway, M. J.; Jayne, J. T.; Aiken, A. C.; Gonin, M.; Fuhrer, K.;
542 Horvath, T.; Docherty, K. S.; Worsnop, D. R.; Jimenez, J. L., Field-deployable, high-resolution, time-of-flight aerosol
543 mass spectrometer. *Anal.Chem.* **2006,** *78*, (24), 8281.

544 35. Canagaratna, M. R.; Jayne, J. T.; Jimenez, J. L.; Allan, J. D.; Alfarra, M. R.; Zhang, Q.; Onasch, T. B.; Drewnick, F.;
545 Coe, H.; Middlebrook, A.; Delia, A.; Williams, L. R.; Trimborn, A. M.; Northway, M. J.; DeCarlo, P. F.; Kolb, C. E.;
546 Davidovits, P.; Worsnop, D. R., Chemical and microphysical characterization of ambient aerosols with the aerodyne
547 aerosol mass spectrometer. *Mass Spectrometry Reviews* **2007,** *26*, (2), 185-222.

548 36. Willis, M. D.; Lee, A. K. Y.; Onasch, T. B.; Fortner, E. C.; Williams, L. R.; Lambe, A. T.; Worsnop, D. R.; Abbatt, J. P.
549 D., Collection efficiency of the soot-particle aerosol mass spectrometer (SP-AMS) for internally mixed particulate black
550 carbon. *Atmospheric Measurement Techniques* **2014,** *7*, (12), 4507-4516.

551 37. Price, D. J.; Chen, C.-L.; Russell, L. M.; Lamjiri, M. A.; Betha, R.; Sanchez, K.; Liu, J.; Lee, A. K. Y.; Cocker, D. R.,
552 More unsaturated, cooking-type hydrocarbon-like organic aerosol particle emissions from renewable diesel compared to
553 ultra low sulfur diesel in at-sea operations of a research vessel. *Aerosol Sci Technol* **2017,** *51*, (2), 135-146.

554 38. Betha, R.; Russell, L. M.; Chen, C.-L.; Liu, J.; Price, D. J.; Sanchez, K. J.; Chen, S.; Lee, A. K. Y.; Collier, S. C.;
555 Zhang, Q.; Zhang, X.; Cappa, C. D., Larger Submicron Particles for Emissions With Residential Burning in Wintertime
556 San Joaquin Valley (Fresno) than for Vehicle Combustion in Summertime South Coast Air Basin (Fontana). *Journal of*
557 *Geophysical Research: Atmospheres* **2018,** *123*, (18), 10,526-10,545.

558 39. Willis, M. D.; Bozem, H.; Kunkel, D.; Lee, A. K. Y.; Schulz, H.; Burkart, J.; Aliabadi, A. A.; Herber, A. B.; Leaitch, W.
559 R.; Abbatt, J. P. D., Aircraft-based measurements of High Arctic springtime aerosol show evidence for vertically
560 varying sources, transport and composition. *Atmos Chem Phys* **2019,** *19*, (1), 57-76.

Author Version

40. Lee, A. K. Y.; Willis, M. D.; Healy, R. M.; Wang, J. M.; Jeong, C. H.; Wenger, J. C.; Evans, G. J.; Abbatt, J. P. D., Single-particle characterization of biomass burning organic aerosol (BBOA): evidence for non-uniform mixing of high molecular weight organics and potassium. *Atmospheric Chemistry and Physics* **2016,** *16*, (9), 5561-5572.

41. Liu, J.; Russell, L. M.; Lee, A. K. Y.; McKinney, K. A.; Surratt, J. D.; Ziemann, P. J., Observational evidence for pollution-influenced selective uptake contributing to biogenic secondary organic aerosols in the southeastern U.S. *Geophys Res Lett* **2017,** *44*, (15), 8056-8064.

42. Liu, P. S. K.; Deng, R.; Smith, K. A.; Williams, L. R.; Jayne, J. T.; Canagaratna, M. R.; Moore, K.; Onasch, T. B.; Worsnop, D. R.; Deshler, T., Transmission Efficiency of an Aerodynamic Focusing Lens System: Comparison of Model Calculations and Laboratory Measurements for the Aerodyne Aerosol Mass Spectrometer. *Aerosol Sci Technol* **2007,** *41*, (8), 721-733.

43. Corbin, J. C.; Sierau, B.; Gysel, M.; Laborde, M.; Keller, A.; Kim, J.; Petzold, A.; Onasch, T. B.; Lohmann, U.; Mensah, A. A., Mass spectrometry of refractory black carbon particles from six sources: carbon-cluster and oxygenated ions. *Atmospheric Chemistry and Physics* **2014,** *14*, (5), 2591-2603.

44. Malmborg, V. B.; Eriksson, A. C.; Shen, M.; Nilsson, P.; Gallo, Y.; Waldheim, B.; Martinsson, J.; Andersson, O.; Pagels, J., Evolution of In-Cylinder Diesel Engine Soot and Emission Characteristics Investigated with Online Aerosol Mass Spectrometry. *Environmental Science & Technology* **2017,** *51*, (3), 1876-1885.

45. Cappa, C. D.; Zhang, X.; Russell, L. M.; Collier, S.; Lee, A. K. Y.; Chen, C.-L.; Betha, R.; Chen, S.; Liu, J.; Price, D. J.; Sanchez, K. J.; McMeeking, G. R.; Williams, L. R.; Onasch, T. B.; Worsnop, D. R.; Abbatt, J.; Zhang, Q., Light Absorption by Ambient Black and Brown Carbon and its Dependence on Black Carbon Coating State for Two California, USA, Cities in Winter and Summer. *Journal of Geophysical Research: Atmospheres* **2019,** *124*, (3), 1550-1577.

46. Fierce, L.; Bond, T. C.; Bauer, S. E.; Mena, F.; Riemer, N., Black carbon absorption at the global scale is affected by particle-scale diversity in composition. *Nature Communications* **2016,** *7*, 12361.

47. Metcalf, A. R.; Loza, C. L.; Coggon, M. M.; Craven, J. S.; Jonsson, H. H.; Flagan, R. C.; Seinfeld, J. H., Secondary Organic Aerosol Coating Formation and Evaporation: Chamber Studies Using Black Carbon Seed Aerosol and the Single-Particle Soot Photometer. *Aerosol Sci Technol* **2013,** *47*, (3), 326-347.

48. Wu, Y.; Cheng, T.; Liu, D.; Allan, J. D.; Zheng, L.; Chen, H., Light Absorption Enhancement of Black Carbon Aerosol Constrained by Particle Morphology. *Environ Sci Technol* **2018,** *52*, (12), 6912-6919.

49. Ahern, A. T.; Subramanian, R.; Saliba, G.; Lipsky, E. M.; Donahue, N. M.; Sullivan, R. C., Effect of secondary organic aerosol coating thickness on the real-time detection and characterization of biomass-burning soot by two particle mass spectrometers. *Atmos. Meas. Tech.* **2016,** *9*, (12), 6117-6137.

50. Ching, J.; Fast, J.; West, M.; Riemer, N., Metrics to quantify the importance of mixing state for CCN activity. *Atmos Chem Phys* **2017,** *17*, (12), 7445-7458.

51. Fierce, L.; Riemer, N.; Bond, T. C., Toward Reduced Representation of Mixing State for Simulating Aerosol Effects on Climate. *Bulletin of the American Meteorological Society* **2017,** *98*, (5), 971-980.

Author Version

Supporting information

Influences of primary emission and secondary coating formation on the particle diversity and mixing state of black carbon particles

Alex K. Y. Lee[1,2*], Laura-Hélèna Rivellini[2], Chia-Li Chen[3 ^], Jun Liu[3], Derek J. Price[3 ǂ], Raghu Betha[3], Lynn M. Russell[3], Xiaolu Zhang[4 #], Christopher D. Cappa[4]

[1]Department of Civil and Environmental Engineering, National University of Singapore, Singapore

[2]NUS Environmental Research Institute, National University of Singapore, Singapore

[3]Scripps Institution of Oceanography, University of California, San Diego, USA

[4]Department of Civil and Environmental Engineering, University of California, Davis, USA

^Now at: Department of Atmospheric Sciences, National Taiwan University, Taipei, Taiwan

[#]Now at: Crocker Nuclear Laboratory, University of California, Davis, USA

[ǂ]Now at: Department of Chemistry and Biochemistry, University of Colorado, Boulder, USA

*Correspondence to: Alex K. Y. Lee (ceelkya@nus.edu.sg)

Table of content:

Text: Single particle detection ...……..Page S2

Text: ETSP data pre-processing and identification of true positive events……..Page S2

Text: Cluster analysis of ETSP events …….Page S3

Figure S1: Segment plot of ETSP events …….Page S4

Figure S2: Scatter plot of total ion signals of individual particle against d_{va} ……...Page S5

Figure S3: Euclidian distanceas a function of number of clusters …….Page S6

Figure S4: Single particle data with correction factor applied …….Page S7

References ……...…Page S8-S9

Single particle detection

This single particle technique has been previously used for investigating sources, atmospheric processing and emission characteristics of aerosol particles.[1-4] The length of data acquisition time for ETSP mode in each 5-min measurement cycle was 2.5 min (i.e., 2.5 min for the ensemble mode). The keys to trigger the detection of specific types of single particle are to define (1) the "Region of Interest" (ROI, an individual or a range of m/z to trigger detection) and (2) the threshold values of each ROI (the minimum number of ions required to save the event). Three ROIs (i.e., the maximum number available in the instrument menu) were used: ROI1: m/z 36, ROI2: m/z 43, and ROI3: m/z 46-150. The threshold values of each ROI were determined using particle-free air on-site, and they were 3, 4, and 5 ions for ROI1, ROI2, and ROI3, respectively. While ROI1 and ROI2 were used to target rBC- and organic-containing particles, respectively, ROI3 could be triggered by the major aerosol components including nitrate, sulfate and organic. For each ETSP event, a total of 8 mass spectra were saved (i.e., 2 before and 5 after the single particle mass spectrum, pre-segment = 2 and post-segment = 5, Figure S1). These additional mass spectra were used to establish the baseline of the signal and to ensure that all mass spectra recorded for the entire particle vaporization plume were saved.

ETSP data pre-processing and identification of true positive events

Tofware (version 2.4.5) was used to pre-process the ETSP raw data and generate input data for identifying real single particle events using a Cluster Input Preparation Panel (CIPP) as previously described.[5] The CIPP has been used to analyze single particle data measured by Aerodyne AMS equipped with a light scattering module [6-9] and has been modified to analyze ETSP measurements.[1-4] The mass spectra in Segment 1 was used as baselines to correct the single particle mass spectra recorded in Segment 2 (Figure S1). The corrected mass spectral matrix was used as an input for CIPP. The total number of ions for each event were calculated as the sum of all ion signals except m/z 14 (N^+), 18 (H_2O^+), 28 (N_2^+), 32 (O_2^+), 40 (Ar^+) due to the strong interferences from air and water. Unlike most of the previous studies, m/z 39 (K^+) was included in the total ion calculation as the tungsten vaporizer (i.e., a major interference of K^+) was removed from the SP-AMS. A simplified version of fragmentation table was used to quantify the ion signals of NR-PM_{rBC} and rBC. The RIE values reported in Lee et al. [10] were used to convert the ion signals to the mass fraction of each chemical component in individual particle. The average number of ions plus

three standard deviations within the two particle-free d_{va} regions (i.e., 10-40 nm and 2000-4000 nm, Figure S2) was calculated to determine the minimum ion threshold for identifying real single particle events within the expected d_{va} region (i.e., 50-1200 nm).[11] The threshold ion value for identifying true single particle event within the particle region was 12.96. The total and real single particle events as a function of d_{va} were presented in Figure S2. The output from CIPP will be used for performing cluster analysis (Section 2.5).

Cluster analysis of ETSP events

Cluster analysis was performed to investigate the mixing state of all the real particles using a Cluster Analysis Panel (CAP) with the built-in k-means algorithm in IGOR Pro (WaveMetrics Inc., version 6).[5, 7, 9] K-means cluster analysis has been used to analyze single particle data measured from Aerodyne AMS-type instruments with a light scattering module.[5-9] Note that k-means clustering can classify ambient particles measured by the aerosol time-of-flight mass spectrometer (ATOFMS, TSI) into particle types that are highly consistent with other clustering algorithms such as ART-2a and hierarchical clustering.[12, 13] Similar to the calculation of total ion signals, m/z 14, 18, 28, 32 and 40 were excluded in the clustering. The fragments of ammonium (m/z 15, 16, 17) and sodium (m/z 23) were also excluded due to the larger measurement uncertainties of these species. All single particle mass spectra were normalized by their total ion signal, and solutions with up to 20 clusters were tested. Euclidian distance was used to evaluate the total distance between the cluster centers and each single particle. In general, increasing the number of clusters can better represent the dataset mathematically as shown in Figure S3. However, a large number of clusters compromises the physical meaning of each cluster. Note that the CAP can also merge multiple clusters into a single particle class if they have similar mass spectral features and size distributions, whereas other clusters remain unchanged.

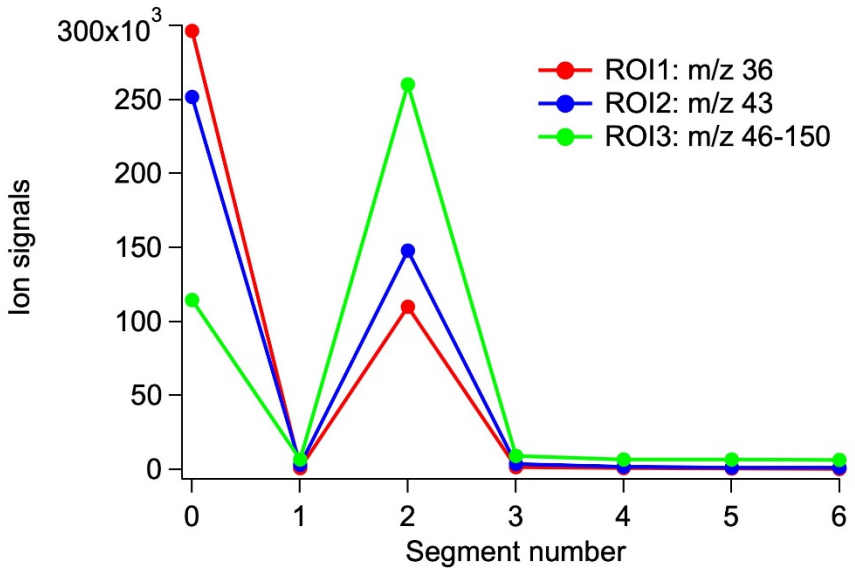

Figure S1: Segment plot of ETSP events. A total of 8 mass spectra were saved (i.e., 2 before and 5 after the single particle mass spectrum, pre-segment = 2 and post-segment = 5). The mass spectral signals in Segment 1 was used as baseline to correct the single particle mass spectra recorded in Segment 2.

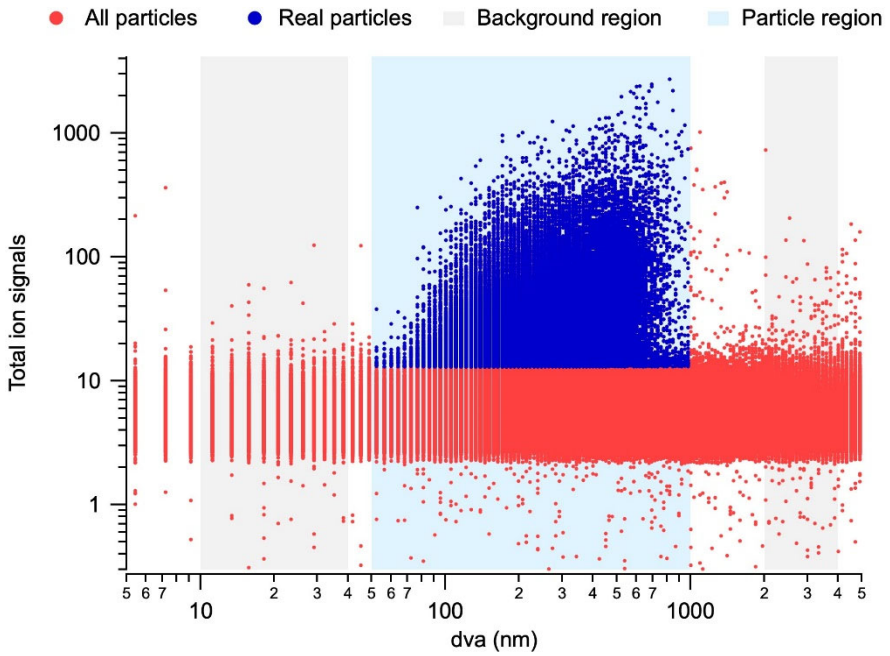

Figure S2: Scatter plot of total ion signals of individual particle against d_{va}. The average number of ions plus three standard deviations within the two particle-free d_{va} regions (i.e., 10-40 nm and 2000-4000 nm, grey regions) was calculated to determine the minimum ion threshold for identifying real single particle events within the expected d_{va} region (i.e., 50-1200 nm). The threshold ion value for identifying true single particle event within the particle region was 12.96. The total and real single particle events were presented in red and blue markers, respectively.

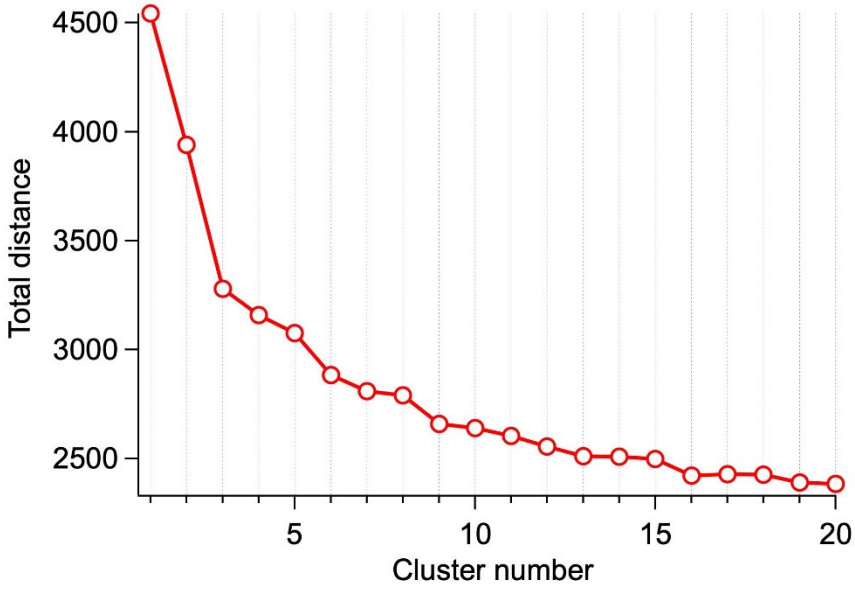

Figure S3: Euclidian distanceas a function of number of clusters. Euclidian distance was used to evaluate the total distance between the cluster centers and each single particle. Increasing the number of clusters can better represent the dataset mathematically

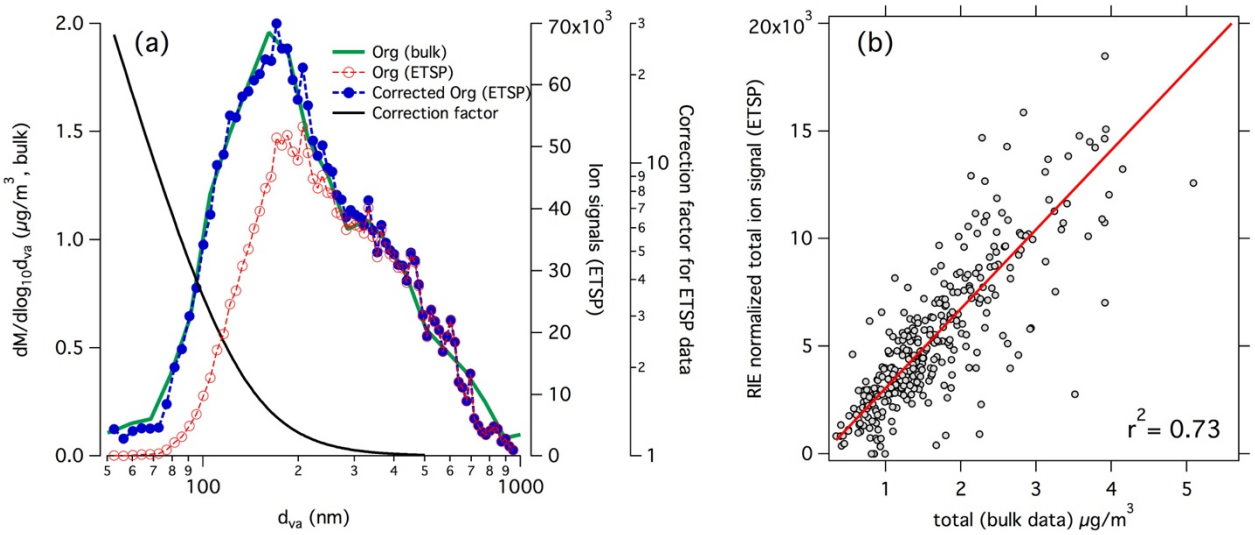

Figure S4: (a) Size distribution of organic: bulk data (green line) and ETSP data with and without correction factor (solid blue circles and open red circles, respectively). (b) Correlation between total mass (i.e., rBC + NR-PM_{rBC}, bulk data) and mass-normalized total ion signal measured by ETSP mode with correction factors applied.

References

1. Price, D. J.; Chen, C.-L.; Russell, L. M.; Lamjiri, M. A.; Betha, R.; Sanchez, K.; Liu, J.; Lee, A. K. Y.; Cocker, D. R., More unsaturated, cooking-type hydrocarbon-like organic aerosol particle emissions from renewable diesel compared to ultra low sulfur diesel in at-sea operations of a research vessel. *Aerosol Sci. Technol.* **2017,** *51*, (2), 135-146.

2. Sanchez, K. J.; Chen, C.-L.; Russell, L. M.; Betha, R.; Liu, J.; Price, D. J.; Massoli, P.; Ziemba, L. D.; Crosbie, E. C.; Moore, R. H.; Müller, M.; Schiller, S. A.; Wisthaler, A.; Lee, A. K. Y.; Quinn, P. K.; Bates, T. S.; Porter, J.; Bell, T. G.; Saltzman, E. S.; Vaillancourt, R. D.; Behrenfeld, M. J., Substantial Seasonal Contribution of Observed Biogenic Sulfate Particles to Cloud Condensation Nuclei. *Sci. Rep.* **2018,** *8*, (1), 3235.

3. Ye, Q.; Gu, P.; Li, H. Z.; Robinson, E. S.; Lipsky, E.; Kaltsonoudis, C.; Lee, A. K. Y.; Apte, J. S.; Robinson, A. L.; Sullivan, R. C.; Presto, A. A.; Donahue, N. M., Spatial Variability of Sources and Mixing State of Atmospheric Particles in a Metropolitan Area. *Environ. Sci. Technol.* **2018,** *52*, (12), 6807-6815.

4. Willis, M. D.; Bozem, H.; Kunkel, D.; Lee, A. K. Y.; Schulz, H.; Burkart, J.; Aliabadi, A. A.; Herber, A. B.; Leaitch, W. R.; Abbatt, J. P. D., Aircraft-based measurements of High Arctic springtime aerosol show evidence for vertically varying sources, transport and composition. *Atmos. Chem. Phys.* **2019,** *19*, (1), 57-76.

5. Lee, A. K. Y.; Willis, M. D.; Healy, R. M.; Onasch, T. B.; Abbatt, J. P. D., Mixing state of carbonaceous aerosol in an urban environment: single particle characterization using the soot particle aerosol mass spectrometer (SP-AMS). *Atmos. Chem. Phys.* **2015,** *15*, (4), 1823-1841.

6. Chen, C.-L.; Chen, S.; Russell, L. M.; Liu, J.; Price, D. J.; Betha, R.; Sanchez, K. J.; Lee, A. K. Y.; Williams, L.; Collier, S. C.; Zhang, Q.; Kumar, A.; Kleeman, M. J.; Zhang, X.; Cappa, C. D., Organic Aerosol Particle Chemical Properties Associated With Residential Burning and Fog in Wintertime San Joaquin Valley (Fresno) and With Vehicle and Firework Emissions in Summertime South Coast Air Basin (Fontana). *J. Geophys. Res.: Atmos.* **2018,** *123*, (18), 10,707-10,731.

7. Lee, A. K. Y.; Willis, M. D.; Healy, R. M.; Wang, J. M.; Jeong, C. H.; Wenger, J. C.; Evans, G. J.; Abbatt, J. P. D., Single-particle characterization of biomass burning organic aerosol (BBOA): evidence for non-uniform mixing of high molecular weight organics and potassium. *Atmos. Chem. Phys.* **2016,** *16*, (9), 5561-5572.

8. Liu, J.; Russell, L. M.; Lee, A. K. Y.; McKinney, K. A.; Surratt, J. D.; Ziemann, P. J., Observational evidence for pollution-influenced selective uptake contributing to biogenic secondary organic aerosols in the southeastern U.S. *Geophys. Res. Lett.* **2017,** *44*, (15), 8056-8064.

9. Willis, M. D.; Healy, R. M.; Riemer, N.; West, M.; Wang, J. M.; Jeong, C. H.; Wenger, J. C.; Evans, G. J.; Abbatt, J. P. D.; Lee, A. K. Y., Quantification of black carbon mixing state from traffic: implications for aerosol optical properties. *Atmos. Chem. Phys.* **2016,** *16*, (7), 4693-4706.

10. Lee, A. K. Y.; Chen, C. L.; Liu, J.; Price, D. J.; Betha, R.; Russell, L. M.; Zhang, X.; Cappa, C. D., Formation of secondary organic aerosol coating on black carbon particles near vehicular emissions. *Atmos. Chem. Phys.* **2017,** *17*, (24), 15055-15067.

11. Liu, P. S. K.; Deng, R.; Smith, K. A.; Williams, L. R.; Jayne, J. T.; Canagaratna, M. R.; Moore, K.; Onasch, T. B.; Worsnop, D. R.; Deshler, T., Transmission Efficiency of an Aerodynamic Focusing Lens System: Comparison of Model Calculations and Laboratory Measurements for the Aerodyne Aerosol Mass Spectrometer. *Aerosol Sci. Technol.* **2007,** *41*, (8), 721-733.

12. Giorio, C.; Tapparo, A.; Dall'Osto, M.; Harrison, R. M.; Beddows, D. C. S.; Di Marco, C.; Nemitz, E., Comparison of three techniques for analysis of data from an Aerosol Time-of-Flight Mass Spectrometer. *Atmos. Environ.* **2012,** *61*, 316-326.

13. Rebotier, T. P.; Prather, K. A., Aerosol time-of-flight mass spectrometry data analysis: A benchmark of clustering algorithms. *Anal. Chim. Acta* **2007,** *585*, (1), 38-54.